

Search for $B^+ \rightarrow D^+ K^0$ and $B^+ \rightarrow D^+ K^{*0}$ decays

P. del Amo Sanchez,¹ J. P. Lees,¹ V. Poireau,¹ E. Prencipe,¹ V. Tisserand,¹ J. Garra Tico,² E. Grauges,² M. Martinelli^{ab,3}, A. Palano^{ab,3}, M. Pappagallo^{ab,3}, G. Eigen,⁴ B. Stugu,⁴ L. Sun,⁴ M. Battaglia,⁵ D. N. Brown,⁵ B. Hooberman,⁵ L. T. Kerth,⁵ Yu. G. Kolomensky,⁵ G. Lynch,⁵ I. L. Osipenko,⁵ T. Tanabe,⁵ C. M. Hawkes,⁶ A. T. Watson,⁶ H. Koch,⁷ T. Schroeder,⁷ D. J. Asgeirsson,⁸ C. Hearty,⁸ T. S. Mattison,⁸ J. A. McKenna,⁸ A. Khan,⁹ A. Randle-Conde,⁹ V. E. Blinov,¹⁰ A. R. Buzykaev,¹⁰ V. P. Druzhinin,¹⁰ V. B. Golubev,¹⁰ A. P. Onuchin,¹⁰ S. I. Serednyakov,¹⁰ Yu. I. Skovpen,¹⁰ E. P. Solodov,¹⁰ K. Yu. Todyshev,¹⁰ A. N. Yushkov,¹⁰ M. Bondioli,¹¹ S. Curry,¹¹ D. Kirkby,¹¹ A. J. Lankford,¹¹ M. Mandelkern,¹¹ E. C. Martin,¹¹ D. P. Stoker,¹¹ H. Atmacan,¹² J. W. Gary,¹² F. Liu,¹² O. Long,¹² G. M. Vitug,¹² C. Campagnari,¹³ T. M. Hong,¹³ D. Kovalskyi,¹³ J. D. Richman,¹³ A. M. Eisner,¹⁴ C. A. Heusch,¹⁴ J. Kroseberg,¹⁴ W. S. Lockman,¹⁴ A. J. Martinez,¹⁴ T. Schalk,¹⁴ B. A. Schumm,¹⁴ A. Seiden,¹⁴ L. O. Winstrom,¹⁴ C. H. Cheng,¹⁵ D. A. Doll,¹⁵ B. Echenard,¹⁵ D. G. Hitlin,¹⁵ P. Ongmongkolkul,¹⁵ F. C. Porter,¹⁵ A. Y. Rakitin,¹⁵ R. Andreassen,¹⁶ M. S. Dubrovin,¹⁶ G. Mancinelli,¹⁶ B. T. Meadows,¹⁶ M. D. Sokoloff,¹⁶ P. C. Bloom,¹⁷ W. T. Ford,¹⁷ A. Gaz,¹⁷ J. F. Hirschauer,¹⁷ M. Nagel,¹⁷ U. Nauenberg,¹⁷ J. G. Smith,¹⁷ S. R. Wagner,¹⁷ R. Ayad,^{18,*} W. H. Toki,¹⁸ T. M. Karbach,¹⁹ J. Merkel,¹⁹ A. Petzold,¹⁹ B. Spaan,¹⁹ K. Wacker,¹⁹ M. J. Kobel,²⁰ K. R. Schubert,²⁰ R. Schwierz,²⁰ D. Bernard,²¹ M. Verderi,²¹ P. J. Clark,²² S. Playfer,²² J. E. Watson,²² M. Andreotti^{ab,23}, D. Bettoni^{a,23}, C. Bozzi^{a,23}, R. Calabrese^{ab,23}, A. Cecchi^{ab,23}, G. Cibinetto^{ab,23}, E. Fioravanti^{ab,23}, P. Franchini^{ab,23}, E. Luppi^{ab,23}, M. Munerato^{ab,23}, M. Negrini^{ab,23}, A. Petrella^{ab,23}, L. Piemontese^{a,23}, R. Baldini-Ferrolì,²⁴ A. Calcaterra,²⁴ R. de Sangro,²⁴ G. Finocchiaro,²⁴ M. Nicolaci,²⁴ S. Pacetti,²⁴ P. Patteri,²⁴ I. M. Peruzzi,^{24,†} M. Piccolo,²⁴ M. Rama,²⁴ A. Zallo,²⁴ R. Contri^{ab,25}, E. Guido^{ab,25}, M. Lo Vetere^{ab,25}, M. R. Monge^{ab,25}, S. Passaggio^{a,25}, C. Patrignani^{ab,25}, E. Robutti^{a,25}, S. Tosi^{ab,25}, B. Bhuyan,²⁶ M. Morii,²⁷ A. Adametz,²⁸ J. Marks,²⁸ S. Schenk,²⁸ U. Uwer,²⁸ F. U. Bernlochner,²⁹ H. M. Lacker,²⁹ T. Lueck,²⁹ A. Volk,²⁹ P. D. Dauncey,³⁰ M. Tibbetts,³⁰ P. K. Behera,³¹ U. Mallik,³¹ C. Chen,³² J. Cochran,³² H. B. Crawley,³² L. Dong,³² W. T. Meyer,³² S. Prell,³² E. I. Rosenberg,³² A. E. Rubin,³² Y. Y. Gao,³³ A. V. Gritsan,³³ Z. J. Guo,³³ N. Arnaud,³⁴ M. Davier,³⁴ D. Derkach,³⁴ J. Firmino da Costa,³⁴ G. Grosdidier,³⁴ F. Le Diberder,³⁴ A. M. Lutz,³⁴ B. Malaescu,³⁴ A. Perez,³⁴ P. Roudeau,³⁴ M. H. Schune,³⁴ J. Serrano,³⁴ V. Sordini,^{34,‡} A. Stocchi,³⁴ L. Wang,³⁴ G. Wormser,³⁴ D. J. Lange,³⁵ D. M. Wright,³⁵ I. Bingham,³⁶ J. P. Burke,³⁶ C. A. Chavez,³⁶ J. P. Coleman,³⁶ J. R. Fry,³⁶ E. Gabathuler,³⁶ R. Gamet,³⁶ D. E. Hutchcroft,³⁶ D. J. Payne,³⁶ C. Touramanis,³⁶ A. J. Bevan,³⁷ F. Di Lodovico,³⁷ R. Sacco,³⁷ M. Sigamani,³⁷ G. Cowan,³⁸ S. Paramesvaran,³⁸ A. C. Wren,³⁸ D. N. Brown,³⁹ C. L. Davis,³⁹ A. G. Denig,⁴⁰ M. Fritsch,⁴⁰ W. Gradl,⁴⁰ A. Hafner,⁴⁰ K. E. Alwyn,⁴¹ D. Bailey,⁴¹ R. J. Barlow,⁴¹ G. Jackson,⁴¹ G. D. Lafferty,⁴¹ T. J. West,⁴¹ J. Anderson,⁴² R. Cenci,⁴² A. Jawahery,⁴² D. A. Roberts,⁴² G. Simi,⁴² J. M. Tuggle,⁴² C. Dallapiccola,⁴³ E. Salvati,⁴³ R. Cowan,⁴⁴ D. Dujmic,⁴⁴ P. H. Fisher,⁴⁴ G. Sciolla,⁴⁴ M. Zhao,⁴⁴ D. Lindemann,⁴⁵ P. M. Patel,⁴⁵ S. H. Robertson,⁴⁵ M. Schram,⁴⁵ P. Biassoni^{ab,46}, A. Lazzaro^{ab,46}, V. Lombardo^{a,46}, F. Palombo^{ab,46}, S. Stracka^{ab,46}, L. Cremaldi,⁴⁷ R. Godang,^{47,§} R. Kroeger,⁴⁷ P. Sonnek,⁴⁷ D. J. Summers,⁴⁷ H. W. Zhao,⁴⁷ X. Nguyen,⁴⁸ M. Simard,⁴⁸ P. Taras,⁴⁸ G. De Nardo^{ab,49}, D. Monorchio^{ab,49}, G. Onorato^{ab,49}, C. Sciacca^{ab,49}, G. Raven,⁵⁰ H. L. Snoek,⁵⁰ C. P. Jessop,⁵¹ K. J. Knoepfel,⁵¹ J. M. LoSecco,⁵¹ W. F. Wang,⁵¹ L. A. Corwin,⁵² K. Honscheid,⁵² R. Kass,⁵² J. P. Morris,⁵² A. M. Rahimi,⁵² N. L. Blount,⁵³ J. Brau,⁵³ R. Frey,⁵³ O. Igonkina,⁵³ J. A. Kolb,⁵³ R. Rahmat,⁵³ N. B. Sinev,⁵³ D. Strom,⁵³ J. Strube,⁵³ E. Torrence,⁵³ G. Castelli^{ab,54}, E. Feltresi^{ab,54}, N. Gagliardi^{ab,54}, M. Margoni^{ab,54}, M. Morandin^{a,54}, M. Posocco^{a,54}, M. Rotondo^{a,54}, F. Simonetto^{ab,54}, R. Stroili^{ab,54}, E. Ben-Haim,⁵⁵ G. R. Bonneaud,⁵⁵ H. Briand,⁵⁵ G. Calderini,⁵⁵ J. Chauveau,⁵⁵ O. Hamon,⁵⁵ Ph. Leruste,⁵⁵ G. Marchiori,⁵⁵ J. Ocariz,⁵⁵ J. Prendki,⁵⁵ S. Sitt,⁵⁵ M. Biasini^{ab,56}, E. Manoni^{ab,56}, C. Angelini^{ab,57}, G. Batignani^{ab,57}, S. Bettarini^{ab,57}, M. Carpinelli^{ab,57,¶}, G. Casarosa^{ab,57}, A. Cervelli^{ab,57}, F. Forti^{ab,57}, M. A. Giorgi^{ab,57}, A. Lusiani^{ac,57}, N. Neri^{ab,57}, E. Paoloni^{ab,57}, G. Rizzo^{ab,57}, J. J. Walsh^{a,57}, D. Lopes Pegna,⁵⁸ C. Lu,⁵⁸ J. Olsen,⁵⁸ A. J. S. Smith,⁵⁸ A. V. Telnov,⁵⁸ F. Anulli^{a,59}, E. Baracchini^{ab,59}, G. Cavoto^{a,59}, R. Faccini^{ab,59}, F. Ferrarotto^{a,59}, F. Ferroni^{ab,59}, M. Gaspero^{ab,59}, L. Li Gioi^{a,59}, M. A. Mazzoni^{a,59}, G. Piredda^{a,59}, F. Renga^{ab,59}, M. Ebert,⁶⁰ T. Hartmann,⁶⁰ T. Leddig,⁶⁰ H. Schröder,⁶⁰ R. Waldi,⁶⁰ T. Adye,⁶¹ B. Franek,⁶¹ E. O. Olaiya,⁶¹ F. F. Wilson,⁶¹ S. Emery,⁶² G. Hamel de Monchenault,⁶² G. Vasseur,⁶² Ch. Yèche,⁶² M. Zito,⁶² M. T. Allen,⁶³ D. Aston,⁶³ D. J. Bard,⁶³ R. Bartoldus,⁶³ J. F. Benitez,⁶³

C. Cartaro,⁶³ M. R. Convery,⁶³ J. Dorfan,⁶³ G. P. Dubois-Felsmann,⁶³ W. Dunwoodie,⁶³ R. C. Field,⁶³ M. Franco Sevilla,⁶³ B. G. Fulsom,⁶³ A. M. Gabareen,⁶³ M. T. Graham,⁶³ P. Grenier,⁶³ C. Hast,⁶³ W. R. Innes,⁶³ M. H. Kelsey,⁶³ H. Kim,⁶³ P. Kim,⁶³ M. L. Kocian,⁶³ D. W. G. S. Leith,⁶³ S. Li,⁶³ B. Lindquist,⁶³ S. Luitz,⁶³ V. Luth,⁶³ H. L. Lynch,⁶³ D. B. MacFarlane,⁶³ H. Marsiske,⁶³ D. R. Muller,⁶³ H. Neal,⁶³ S. Nelson,⁶³ C. P. O'Grady,⁶³ I. Ofte,⁶³ M. Perl,⁶³ T. Pulliam,⁶³ B. N. Ratcliff,⁶³ A. Roodman,⁶³ A. A. Salnikov,⁶³ V. Santoro,⁶³ R. H. Schindler,⁶³ J. Schwiening,⁶³ A. Snyder,⁶³ D. Su,⁶³ M. K. Sullivan,⁶³ S. Sun,⁶³ K. Suzuki,⁶³ J. M. Thompson,⁶³ J. Va'vra,⁶³ A. P. Wagner,⁶³ M. Weaver,⁶³ C. A. West,⁶³ W. J. Wisniewski,⁶³ M. Wittgen,⁶³ D. H. Wright,⁶³ H. W. Wulsin,⁶³ A. K. Yarritu,⁶³ C. C. Young,⁶³ V. Ziegler,⁶³ X. R. Chen,⁶⁴ W. Park,⁶⁴ M. V. Purohit,⁶⁴ R. M. White,⁶⁴ J. R. Wilson,⁶⁴ S. J. Sekula,⁶⁵ M. Bellis,⁶⁶ P. R. Burchat,⁶⁶ A. J. Edwards,⁶⁶ T. S. Miyashita,⁶⁶ S. Ahmed,⁶⁷ M. S. Alam,⁶⁷ J. A. Ernst,⁶⁷ B. Pan,⁶⁷ M. A. Saeed,⁶⁷ S. B. Zain,⁶⁷ N. Guttman,⁶⁸ A. Soffer,⁶⁸ P. Lund,⁶⁹ S. M. Spanier,⁶⁹ R. Eckmann,⁷⁰ J. L. Ritchie,⁷⁰ A. M. Ruland,⁷⁰ C. J. Schilling,⁷⁰ R. F. Schwitters,⁷⁰ B. C. Wray,⁷⁰ J. M. Izen,⁷¹ X. C. Lou,⁷¹ F. Bianchi^{ab},⁷² D. Gamba^{ab},⁷² M. Pelliccioni^{ab},⁷² M. Bomben^{ab},⁷³ L. Lanceri^{ab},⁷³ L. Vitale^{ab},⁷³ N. Lopez-March,⁷⁴ F. Martinez-Vidal,⁷⁴ D. A. Milanese,⁷⁴ A. Oyangueren,⁷⁴ J. Albert,⁷⁵ Sw. Banerjee,⁷⁵ H. H. F. Choi,⁷⁵ K. Hamano,⁷⁵ G. J. King,⁷⁵ R. Kowalewski,⁷⁵ M. J. Lewczuk,⁷⁵ I. M. Nugent,⁷⁵ J. M. Roney,⁷⁵ R. J. Sobie,⁷⁵ T. J. Gershon,⁷⁶ P. F. Harrison,⁷⁶ J. Ilic,⁷⁶ T. E. Latham,⁷⁶ E. M. T. Puccio,⁷⁶ H. R. Band,⁷⁷ X. Chen,⁷⁷ S. Dasu,⁷⁷ K. T. Flood,⁷⁷ Y. Pan,⁷⁷ R. Prepost,⁷⁷ C. O. Vuosalo,⁷⁷ and S. L. Wu⁷⁷

¹Laboratoire d'Annecy-le-Vieux de Physique des Particules (LAPP),
Université de Savoie, CNRS/IN2P3, F-74941 Annecy-Le-Vieux, France

²Universitat de Barcelona, Facultat de Física, Departament ECM, E-08028 Barcelona, Spain

³INFN Sezione di Bari^a; Dipartimento di Fisica, Università di Bari^b, I-70126 Bari, Italy

⁴University of Bergen, Institute of Physics, N-5007 Bergen, Norway

⁵Lawrence Berkeley National Laboratory and University of California, Berkeley, California 94720, USA

⁶University of Birmingham, Birmingham, B15 2TT, United Kingdom

⁷Ruhr Universität Bochum, Institut für Experimentalphysik 1, D-44780 Bochum, Germany

⁸University of British Columbia, Vancouver, British Columbia, Canada V6T 1Z1

⁹Brunel University, Uxbridge, Middlesex UB8 3PH, United Kingdom

¹⁰Budker Institute of Nuclear Physics, Novosibirsk 630090, Russia

¹¹University of California at Irvine, Irvine, California 92697, USA

¹²University of California at Riverside, Riverside, California 92521, USA

¹³University of California at Santa Barbara, Santa Barbara, California 93106, USA

¹⁴University of California at Santa Cruz, Institute for Particle Physics, Santa Cruz, California 95064, USA

¹⁵California Institute of Technology, Pasadena, California 91125, USA

¹⁶University of Cincinnati, Cincinnati, Ohio 45221, USA

¹⁷University of Colorado, Boulder, Colorado 80309, USA

¹⁸Colorado State University, Fort Collins, Colorado 80523, USA

¹⁹Technische Universität Dortmund, Fakultät Physik, D-44221 Dortmund, Germany

²⁰Technische Universität Dresden, Institut für Kern- und Teilchenphysik, D-01062 Dresden, Germany

²¹Laboratoire Leprince-Ringuet, CNRS/IN2P3, Ecole Polytechnique, F-91128 Palaiseau, France

²²University of Edinburgh, Edinburgh EH9 3JZ, United Kingdom

²³INFN Sezione di Ferrara^a; Dipartimento di Fisica, Università di Ferrara^b, I-44100 Ferrara, Italy

²⁴INFN Laboratori Nazionali di Frascati, I-00044 Frascati, Italy

²⁵INFN Sezione di Genova^a; Dipartimento di Fisica, Università di Genova^b, I-16146 Genova, Italy

²⁶Indian Institute of Technology Guwahati, Guwahati, Assam, 781 039, India

²⁷Harvard University, Cambridge, Massachusetts 02138, USA

²⁸Universität Heidelberg, Physikalisches Institut, Philosophenweg 12, D-69120 Heidelberg, Germany

²⁹Humboldt-Universität zu Berlin, Institut für Physik, Newtonstr. 15, D-12489 Berlin, Germany

³⁰Imperial College London, London, SW7 2AZ, United Kingdom

³¹University of Iowa, Iowa City, Iowa 52242, USA

³²Iowa State University, Ames, Iowa 50011-3160, USA

³³Johns Hopkins University, Baltimore, Maryland 21218, USA

³⁴Laboratoire de l'Accélérateur Linéaire, IN2P3/CNRS et Université Paris-Sud 11,

Centre Scientifique d'Orsay, B. P. 34, F-91898 Orsay Cedex, France

³⁵Lawrence Livermore National Laboratory, Livermore, California 94550, USA

³⁶University of Liverpool, Liverpool L69 7ZE, United Kingdom

³⁷Queen Mary, University of London, London, E1 4NS, United Kingdom

³⁸University of London, Royal Holloway and Bedford New College, Egham, Surrey TW20 0EX, United Kingdom

³⁹University of Louisville, Louisville, Kentucky 40292, USA

⁴⁰Johannes Gutenberg-Universität Mainz, Institut für Kernphysik, D-55099 Mainz, Germany

⁴¹University of Manchester, Manchester M13 9PL, United Kingdom

⁴²University of Maryland, College Park, Maryland 20742, USA

- ⁴³University of Massachusetts, Amherst, Massachusetts 01003, USA
- ⁴⁴Massachusetts Institute of Technology, Laboratory for Nuclear Science, Cambridge, Massachusetts 02139, USA
- ⁴⁵McGill University, Montréal, Québec, Canada H3A 2T8
- ⁴⁶INFN Sezione di Milano^a; Dipartimento di Fisica, Università di Milano^b, I-20133 Milano, Italy
- ⁴⁷University of Mississippi, University, Mississippi 38677, USA
- ⁴⁸Université de Montréal, Physique des Particules, Montréal, Québec, Canada H3C 3J7
- ⁴⁹INFN Sezione di Napoli^a; Dipartimento di Scienze Fisiche, Università di Napoli Federico II^b, I-80126 Napoli, Italy
- ⁵⁰NIKHEF, National Institute for Nuclear Physics and High Energy Physics, NL-1009 DB Amsterdam, The Netherlands
- ⁵¹University of Notre Dame, Notre Dame, Indiana 46556, USA
- ⁵²Ohio State University, Columbus, Ohio 43210, USA
- ⁵³University of Oregon, Eugene, Oregon 97403, USA
- ⁵⁴INFN Sezione di Padova^a; Dipartimento di Fisica, Università di Padova^b, I-35131 Padova, Italy
- ⁵⁵Laboratoire de Physique Nucléaire et de Hautes Energies, IN2P3/CNRS, Université Pierre et Marie Curie-Paris6, Université Denis Diderot-Paris7, F-75252 Paris, France
- ⁵⁶INFN Sezione di Perugia^a; Dipartimento di Fisica, Università di Perugia^b, I-06100 Perugia, Italy
- ⁵⁷INFN Sezione di Pisa^a; Dipartimento di Fisica, Università di Pisa^b; Scuola Normale Superiore di Pisa^c, I-56127 Pisa, Italy
- ⁵⁸Princeton University, Princeton, New Jersey 08544, USA
- ⁵⁹INFN Sezione di Roma^a; Dipartimento di Fisica, Università di Roma La Sapienza^b, I-00185 Roma, Italy
- ⁶⁰Universität Rostock, D-18051 Rostock, Germany
- ⁶¹Rutherford Appleton Laboratory, Chilton, Didcot, Oxon, OX11 0QX, United Kingdom
- ⁶²CEA, Irfu, SPP, Centre de Saclay, F-91191 Gif-sur-Yvette, France
- ⁶³SLAC National Accelerator Laboratory, Stanford, California 94309 USA
- ⁶⁴University of South Carolina, Columbia, South Carolina 29208, USA
- ⁶⁵Southern Methodist University, Dallas, Texas 75275, USA
- ⁶⁶Stanford University, Stanford, California 94305-4060, USA
- ⁶⁷State University of New York, Albany, New York 12222, USA
- ⁶⁸Tel Aviv University, School of Physics and Astronomy, Tel Aviv, 69978, Israel
- ⁶⁹University of Tennessee, Knoxville, Tennessee 37996, USA
- ⁷⁰University of Texas at Austin, Austin, Texas 78712, USA
- ⁷¹University of Texas at Dallas, Richardson, Texas 75083, USA
- ⁷²INFN Sezione di Torino^a; Dipartimento di Fisica Sperimentale, Università di Torino^b, I-10125 Torino, Italy
- ⁷³INFN Sezione di Trieste^a; Dipartimento di Fisica, Università di Trieste^b, I-34127 Trieste, Italy
- ⁷⁴IFIC, Universitat de Valencia-CSIC, E-46071 Valencia, Spain
- ⁷⁵University of Victoria, Victoria, British Columbia, Canada V8W 3P6
- ⁷⁶Department of Physics, University of Warwick, Coventry CV4 7AL, United Kingdom
- ⁷⁷University of Wisconsin, Madison, Wisconsin 53706, USA

We report a search for the rare decays $B^+ \rightarrow D^+ K^0$ and $B^+ \rightarrow D^+ K^{*0}$ in an event sample of approximately 465 million $B\bar{B}$ pairs collected with the BABAR detector at the PEP-II asymmetric-energy e^+e^- collider at SLAC. We find no significant evidence for either mode and we set 90% probability upper limits on the branching fractions of $\mathcal{B}(B^+ \rightarrow D^+ K^0) < 2.9 \times 10^{-6}$ and $\mathcal{B}(B^+ \rightarrow D^+ K^{*0}) < 3.0 \times 10^{-6}$.

PACS numbers: 13.25.Hw, 14.40.Nd

INTRODUCTION

Charged B meson decays in which neither constituent quark appears in the final state, such as $B^+ \rightarrow D^+ K^{(*)0}$, are expected to be dominated by weak annihilation diagrams with the $\bar{b}u$ pair annihilating into a W^+ boson. Such processes therefore can provide insight into the internal dynamics of B mesons, in particular the overlap between the b and the u quark wave functions. Annihilation amplitudes cannot be evaluated with the commonly used factorization approach [1]. As a consequence, there are no reliable estimates for the corresponding decay

rates. Annihilation amplitudes are expected to be proportional to f_B/m_B where m_B is the mass of the B meson and f_B is the pseudoscalar B meson decay constant. The quantity f_B represents the probability amplitude for the two quark wave functions to overlap. Numerically, f_B/m_B is approximately equal to λ^2 , where λ is the sine of the Cabibbo angle [1, 2]. In addition, these amplitudes are also suppressed by the CKM factor $|V_{ub}| \sim \lambda^3$. So far, there has been no observation of a hadronic B meson decay that proceeds purely through weak annihilation diagrams, although evidence for the leptonic decay $B \rightarrow \tau\nu$ has been found [3]. In theoretical calculations

of nonleptonic decays, the assumption is often made that these amplitudes may be neglected.

Some studies indicate that the branching fractions of weak-annihilation processes could be enhanced by so-called rescattering effects, in which long-range strong interactions between B decay products, rather than the decay amplitudes, lead to the final state of interest [2]. Figure 1 shows the Feynman diagram for the decays $B^+ \rightarrow D^+ K^{(*)0}$ and $B^+ \rightarrow D_s^+ \pi^0$ [4], and the hadron-level diagram for the rescattering of $D_s^+ \pi^0$ into $D^+ K^{(*)0}$. Significant rescattering could thus mimic a large weak annihilation amplitude. It has been argued [2] that rescattering effects might be suppressed by only λ^4 , compared to λ^5 for the weak annihilation amplitudes, rendering the $B^+ \rightarrow D^+ K^{(*)0}$ decay rate due to rescattering comparable to the isospin-related color-suppressed $B^0 \rightarrow D^0 K^{(*)0}$ decay rate of approximately 5×10^{-6} .

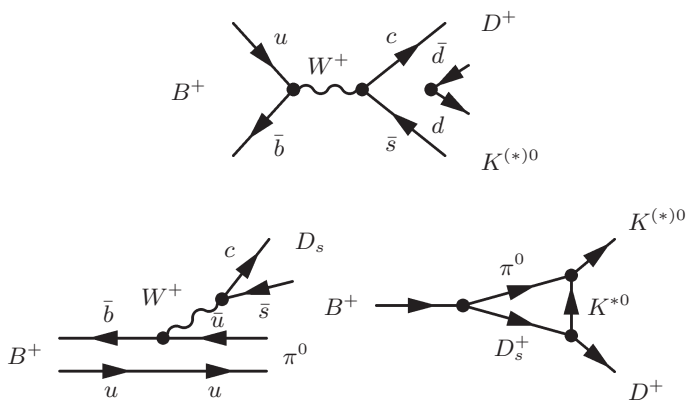


FIG. 1: Annihilation diagram for the decay $B^+ \rightarrow D^+ K^{(*)0}$ (top). Tree diagram (bottom left) for the decay $B^+ \rightarrow D_s^+ \pi^0$ and hadron-level diagram (bottom right) for the rescattering contribution to $B^+ \rightarrow D^+ K^{(*)0}$ via $B^+ \rightarrow D_s^+ \pi^0$.

$B^+ \rightarrow D^+ K^{(*)0}$ decays are also of interest because their decay rates can be used to constrain the annihilation amplitudes in phenomenological fits [1, 5]. This allows the translation of the measurements of the $B^+ \rightarrow D^0 K^{(*)+}$ amplitudes into estimations of the $|V_{ub}|$ suppressed amplitudes $B^0 \rightarrow D^0 K^{(*)0}$ [5, 6]. None of the modes studied here has been observed so far, and a 90% confidence level upper limit on the branching fraction $\mathcal{B}(B^+ \rightarrow D^+ K^0) < 5 \times 10^{-6}$ has been established by *BABAR* [7]. No study of $B^+ \rightarrow D^+ K^{*0}$ has previously been published.

The results presented here are obtained with 426 fb^{-1} of data collected at the $\Upsilon(4S)$ resonance with the *BABAR* detector at the PEP-II asymmetric e^+e^- collider [9] corresponding to 465×10^6 $B\bar{B}$ pairs ($N_{B\bar{B}}$). An additional 44.4 fb^{-1} of data (“off-resonance”) collected at a center-of-mass (CM) energy 40 MeV below the $\Upsilon(4S)$

resonance is used to study backgrounds from $e^+e^- \rightarrow q\bar{q}$ ($q = u, d, s, \text{ or } c$) processes, which we refer to as continuum events.

The *BABAR* detector is described in detail elsewhere [10]. Charged-particle tracking is provided by a five layer silicon vertex tracker (SVT) and a 40 layer drift chamber (DCH). In addition to providing precise position information for tracking, the SVT and DCH measure the specific ionization, which is used for particle identification of low-momentum charged particles. At higher momenta ($p > 0.7 \text{ GeV}/c$) pions and kaons are identified by Cherenkov radiation detected in a ring-imaging device (DIRC). The position and energy of photons are measured with an electromagnetic calorimeter (EMC) consisting of 6580 thallium-doped CsI crystals. These systems are mounted inside a 1.5 T solenoidal superconducting magnet. Muons are identified by the instrumented magnetic-flux return, which is located outside the magnet.

EVENT RECONSTRUCTION AND SELECTION

The event selection criteria are determined using Monte Carlo (MC) simulations of $e^+e^- \rightarrow \Upsilon(4S) \rightarrow B\bar{B}$ (“ $B\bar{B}$ ” in the following) and continuum events, and the off-resonance data. The selection criteria are optimized by maximizing the quantity $S/\sqrt{S+B}$, where S and B are the expected numbers of signal and background events, respectively. We assume the signal branching fraction to be 5×10^{-6} in the optimization procedure.

The charged particle candidates are required to have transverse momenta above 100 MeV/ c and at least twelve hits in the DCH.

Candidate D^+ mesons are reconstructed in the $D^+ \rightarrow K^-\pi^+\pi^+$ ($K\pi\pi$ in the following), $D^+ \rightarrow K_s^0\pi^+$ ($K_s^0\pi$), $D^+ \rightarrow K^-\pi^+\pi^+\pi^0$ ($K\pi\pi\pi^0$) and $D^+ \rightarrow K_s^0\pi^+\pi^0$ ($K_s^0\pi\pi^0$) modes for the $B^+ \rightarrow D^+K^0$ decay channel (DK). Only the first two modes are used for the $B^+ \rightarrow D^+K^{*0}$ decay channel (DK^* in the following) since we find that including the $K\pi\pi\pi^0$ and $K_s^0\pi\pi^0$ modes in this channel does not appreciably improve the sensitivity of the analysis.

The D^+ candidates are reconstructed by combining kaons (either charged or neutral depending on the channel) and the appropriate number of pions. The charged kaons used to reconstruct the D^+ and K^{*0} candidates are required to satisfy kaon identification criteria obtained using a likelihood technique based on the opening angle of the Cherenkov light measured in the DIRC and the ionization energy loss measured in the SVT and DCH. These criteria are typically 85% efficient, depending on the momentum and polar angle, with misidentification rates at the 2% level. Kaons and pions from D decays are required to have momenta in the laboratory frame greater than 200 MeV/ c and 150 MeV/ c , respectively.

The reconstructed D^+ candidates are required to satisfy the invariant mass (M_D) selection criteria given in Table I.

The K_s^0 candidates are reconstructed from pairs of oppositely-charged pions with invariant mass within 5–7 MeV/ c^2 of the nominal K_s^0 mass [11]. This mass cut corresponds to 2–2.8 standard deviations of the experimental resolution and varies slightly among channels due to the different amounts of background per channel. For the prompt K_s^0 candidates from the $B^+ \rightarrow D^+ K_s^0$ decay, we require $1 - \cos \alpha_{K_s^0}(B^+) < 10^{-8}$, where $\alpha_{K_s^0}(B^+)$ is the angle between the momentum vector of the K_s^0 candidate and the vector connecting the B^+ and K_s^0 decay vertices. For K_s^0 daughters of a D^+ decay, we require $1 - \cos \alpha_{K_s^0}(D^+) < 10^{-6}$, where $\alpha_{K_s^0}(D^+)$ is defined in a similar way.

The π^0 candidates are reconstructed from pairs of photon candidates each with an energy greater than 70 MeV, and a lateral shower profile in the EMC consistent with a single electromagnetic deposit. These pairs must have a total energy greater than 200 MeV, a CM momentum greater than 400 MeV/ c , and an invariant mass within 10 MeV/ c^2 (for the $K\pi\pi\pi^0$ mode) or 12 MeV/ c^2 (for the $K_s^0\pi\pi^0$ mode) of the nominal π^0 mass [11].

The K^{*0} candidates are reconstructed in the decay channel $K^{*0} \rightarrow K^+\pi^-$. These charged tracks are constrained to originate from a common vertex. The reconstructed invariant mass, whose width is dominated by the K^{*0} natural width, is required to lie within 40 MeV/ c^2 of the nominal K^{*0} mass [11]. We define θ_H as the angle between the direction of flight of the charged K and the direction of flight of the B in the K^{*0} rest frame. The probability distribution of $\cos \theta_H$ is proportional to $\cos^2 \theta_H$ for longitudinally polarized K^{*0} mesons from $B \rightarrow DK^{*0}$ decays, due to angular momentum conservation, and is approximately flat for fake (random combinations of tracks) or unpolarized background K^{*0} candidates. To suppress fake and background K^{*0} candidates we require $|\cos \theta_H| > 0.5$.

The B^+ candidates are reconstructed by combining one D^+ and one K_s^0 or K^{*0} candidate, constraining them to originate from a common vertex. The probability distribution of the cosine of the B polar angle with respect to the beam axis in the CM frame, $\cos \theta_B$, is expected to be proportional to $1 - \cos^2 \theta_B$. Selection criteria on $|\cos \theta_B|$ are channel dependent and are summarized in Table I.

We measure two almost independent kinematic variables: the beam-energy substituted mass $m_{\text{ES}} \equiv \sqrt{(E_0^{*2}/2 + \vec{p}_0 \cdot \vec{p}_B)^2/E_0^2 - p_B^2}$, and the energy difference $\Delta E \equiv E_B^* - E_0^*/2$, where E and p are energy and momentum, the subscripts B and 0 refer to the candidate B and to the e^+e^- system, respectively, and the asterisk denotes a calculation made in the CM frame. Signal events are expected to peak at the B meson mass for m_{ES} and at zero for ΔE . Channel-dependent selection criteria

on $|\Delta E|$ are given in Table I. We retain candidates with m_{ES} in the range [5.20, 5.29] GeV/ c^2 for subsequent analysis.

In less than 1% of the cases, multiple B^+ candidates are present in the same event, and in those cases we choose the one with the reconstructed D^+ mass closest to the nominal mass value [11]. If more than one B^+ candidate shares the same D^+ candidate, then we choose the B^+ candidate with ΔE closest to zero.

BACKGROUND CHARACTERIZATION

After applying the selection criteria described above, the remaining background is composed of non-signal $B\bar{B}$ events and continuum events, the latter being the dominant contribution. Continuum background events, in contrast to $B\bar{B}$ events, are characterized by a jet-like shape, which can be used in a Fisher discriminant \mathcal{F} [12] to reduce this background component. The discriminant \mathcal{F} is a linear combination of four variables trained to peak at 1 for signal and at -1 for continuum background. The first variable is the cosine of the angle between the B thrust axis and the thrust axis of all the other reconstructed charged tracks and neutral energy deposits (rest of the event), where the thrust axis is defined as the direction that maximizes the sum of the longitudinal momenta of all the particles. The second and third variables are the event shape moments $L_0 = \sum_i p_i$, and $L_2 = \sum_i p_i |\cos \theta_i|^2$, where the index i runs over all tracks and energy deposits in the rest of the event; p_i is the momentum and θ_i is the angle with respect to the thrust axis of the B candidate. These three variables are calculated in the CM. Finally we use $|\Delta t|$, the absolute value of the measured proper time interval between the two B decays [8]. It is calculated using the measured separation along the beam direction Δz between the decay points of the reconstructed B and the other B and the Lorentz boost between the laboratory and CM frames. The other B decay point is obtained from the tracks that do not belong to the reconstructed B , with constraints from the reconstructed B momentum and the beam-spot location. The coefficients of \mathcal{F} , chosen to maximize the separation between signal and continuum background, are determined with samples of simulated signal and continuum events, and validated using off-resonance data. We denote two regions: the fit region, defined as $5.20 < m_{\text{ES}} < 5.29$ GeV/ c^2 and $-5 < \mathcal{F} < 5$, and the signal region, defined as $5.27 < m_{\text{ES}} < 5.29$ GeV/ c^2 and $0 < \mathcal{F} < 5$.

To reduce the importance of the continuum background in the final sample we divide the events according to their flavor-tagging category [8]. We define the following exclusive tagging categories:

- *lepton category*, events contain at least one lepton

TABLE I: Main selection criteria used to distinguish between signal and background events. $M_{D, \text{PDG}}$ is the nominal mass of the D^+ meson [11].

Selection criteria	$B^+ \rightarrow D^+ K^0$				$B^+ \rightarrow D^+ K^{*0}$	
	$K\pi\pi$	$K\pi\pi\pi^0$	$K_S^0\pi$	$K_S^0\pi\pi^0$	$K\pi\pi$	$K_S^0\pi$
$ M_{D, \text{PDG}} $ (MeV/ c^2)	<12 ($\simeq 1.9\sigma$)	<18 ($\simeq 1.5\sigma$)	<14 ($\simeq 1.6\sigma$)	<22 ($\simeq 1.6\sigma$)	<10 ($\simeq 1.6\sigma$)	<10 ($\simeq 1.8\sigma$)
$ \cos\theta_B $	<0.76	<0.77	<0.87	<0.85	<0.82	<0.84
$ \Delta E $ (MeV)	<20 ($\simeq 1.3\sigma$)	<23 ($\simeq 1.5\sigma$)	<25 ($\simeq 1.5\sigma$)	<24 ($\simeq 1.5\sigma$)	<19 ($\simeq 1.3\sigma$)	<19 MeV ($\simeq 1.3\sigma$)

TABLE II: Reconstruction efficiencies and expected numbers of events in the fit and signal region assuming $\mathcal{B}(B^+ \rightarrow D^+ K^0) = \mathcal{B}(B^+ \rightarrow D^+ K^{*0}) = 5 \times 10^{-6}$.

	region	$B^+ \rightarrow D^+ K^0$				$B^+ \rightarrow D^+ K^{*0}$	
		$K\pi\pi$	$K\pi\pi\pi^0$	$K_S^0\pi$	$K_S^0\pi\pi^0$	$K\pi\pi$	$K_S^0\pi$
Signal efficiency	fit	18.4%	5.2%	21.3%	6.2%	10.6%	10.5%
	signal	12.4%	3.8%	14.7%	4.9%	7.6%	7.4%
Signal	fit	14.1 ± 0.2	2.5 ± 0.1	1.81 ± 0.03	2.4 ± 0.1	15.8 ± 0.3	1.70 ± 0.04
	signal	9.6 ± 0.2	1.8 ± 0.1	1.21 ± 0.03	1.9 ± 0.1	11.3 ± 0.3	1.20 ± 0.03
Combinatorial $B\bar{B}$ background	fit	67 ± 4	157 ± 4	12 ± 2	36 ± 3	400 ± 10	42.8 ± 4
	signal	7 ± 2	20 ± 2	3 ± 1	8 ± 2	30 ± 2	6.4 ± 1
Peaking $B\bar{B}$ background	fit	2.0 ± 0.2	3.3 ± 0.4	1.1 ± 0.2	1.8 ± 0.5	26 ± 2	2.4 ± 0.3
	signal	0.3 ± 0.1	1.0 ± 0.2	0.3 ± 0.1	0.6 ± 0.2	5.4 ± 1	0.7 ± 0.2
Continuum background	fit	2840 ± 40	4860 ± 50	640 ± 20	1600 ± 30	6100 ± 50	630 ± 20
	signal	63 ± 6	104 ± 8	12 ± 3	45 ± 5	129 ± 8	13 ± 3

in the decay of the other B meson;

- *kaon category*, events contain at least one kaon in the decay of the other B meson, which do not belong to the first category;
- *other category* contains all the events not included in the two previous categories.

The first two categories are expected to be less contaminated by continuum background. We fit all three categories simultaneously. Studies of simulated events show that using the tagging categories reduces the statistical uncertainty on the measured branching fraction for the $K\pi\pi$ mode by 5%, but leads to little gain for the other modes (which are less statistically significant themselves). Hence, we use tagging information only for the $K\pi\pi$ channel.

The $B\bar{B}$ background is divided into two components: non-peaking (combinatorial) and peaking. The latter can occur when one or several particles of a background channel are replaced by a low momentum charged π^+ and the resulting candidate still contributes to the signal region. The largest contributions to the $B\bar{B}$ peaking background for the $B^+ \rightarrow D^+ K^0$ channel arise from the following decays: $\bar{B}^0 \rightarrow D^+ \rho^-$ with D^+ decaying into signal channels, $B^0 \rightarrow \bar{D}^0 K^0$ and $B^0 \rightarrow \bar{D}^{*0} K^0$. To further reduce the contribution from the $\bar{B}^0 \rightarrow D^+ \rho^-$ background, the variable $|\cos\theta_{K_S^0}|$ has been introduced, where $\theta_{K_S^0}$ is the K_S^0 helicity angle, i.e., the angle between one of the two pions from the K_S^0 and the D^+ in the K_S^0 rest frame. We

reject events with $|\cos\theta_{K_S^0}|$ greater than 0.8 for the $K\pi\pi$ mode and 0.9 for all other modes. Based on MC studies, we expect no more than 1 $B\bar{B}$ peaking background event per mode in the signal region, after applying all selection criteria (see Table II). A similar study is performed for the $B^+ \rightarrow D^+ K^{*0}$ decay modes. The main peaking backgrounds arise from $\bar{B}^0 \rightarrow D^+ \rho^-$, $\bar{B}^0 \rightarrow D^+ K^{*-}$, and $\bar{B}^0 \rightarrow D^+ a_1^-$. In all cases, the D^+ decays into the signal decay modes. The number of $B\bar{B}$ peaking background events expected in the signal region for the DK^* mode are shown in Table II.

Charmless B decays may also contribute to the peaking background. These decays can produce π and K mesons with characteristics similar to those of signal events without forming a real D meson. The charmless background is evaluated from data using the D^+ sidebands: events are required to satisfy the criteria $1.774 < M_D < 1.840$ GeV/ c^2 or $1.900 < M_D < 1.954$ GeV/ c^2 . We obtain -1.7 ± 1.0 events for DK decays and -0.7 ± 2.1 events for DK^* decays. We estimate the charmless peaking background contribution to be negligible and assign a systematic uncertainty based on this assumption.

The overall reconstruction and selection efficiencies for signal events, as well as the numbers of expected events for each background category, are given in Table II.

TABLE III: Expected errors on the branching fractions from toy MC studies depending on the branching fractions generated. The combined errors are obtained as results of likelihood combination per each toy (see text for details). All the numbers are given in units of 10^{-6} .

Decay mode	$\mathcal{B} = 5$		$\mathcal{B} = 0$	
	Mean error	[95% range]	Mean error	[95% range]
$B^+ \rightarrow D^+ K^0$				
$K\pi\pi$	+3.3	[2.7, 4.0]	+2.8	[2.2, 3.6]
	-3.0	[2.2, 3.6]	-2.4	[1.6, 3.2]
$K\pi\pi\pi^0$	+20	[14, 25]	+19	[13, 24]
	-17	[10, 23]	-17	[9.4, 22]
$K_S^0\pi$	+12	[7.3, 16]	+11	[7.1, 16]
	-8	[4.6, 14]	-8	[4.5, 14]
$K_S^0\pi\pi^0$	+14	[8.9, 18]	+13	[8.3, 17]
	-12	[6.2, 16]	-11	[5.6, 15]
combined	± 2.9	[2.1, 3.6]	± 2.5	[1.5, 3.2]
$B^+ \rightarrow D^+ K^{*0}$				
$K\pi\pi$	+3.5	[2.5, 4.0]	+3.3	[2.5, 4.0]
	-3.2	[1.8, 3.6]	-2.8	[1.6, 3.8]
$K_S^0\pi$	+15	[9.8, 19]	+14	[7.9, 17]
	-11	[5.8, 16]	-7.7	[3.8, 14]
combined	± 3.3	[2.1, 4.2]	± 3.0	[1.8, 3.9]

TABLE IV: Branching fraction fit results in units of 10^{-6} , with statistical uncertainties. N_i are the yields of the fitted species, and \mathcal{B} represents the calculated branching fraction for each channel.

Decay mode	N_{sig}	$N_{B\bar{B}}$	N_{cont}	\mathcal{B}
$B^+ \rightarrow D^+ K^0$				
$K\pi\pi$	$-11.9^{+6.7}_{-5.6}$	70 ± 27	2690 ± 57	$-4.2^{+2.4}_{-2.0}$
$K\pi\pi\pi^0$	10^{+10}_{-9}	111 ± 51	6516 ± 94	20^{+20}_{-17}
$K_S^0\pi$	$0.6^{+5.3}_{-4.5}$	20 ± 14	381 ± 23	0.7^{+15}_{-13}
$K_S^0\pi\pi^0$	$-6.7^{+4.5}_{-2.8}$	36 ± 22	1270 ± 41	$-14^{+9.2}_{-6.2}$
combined	-	-	-	$-3.4^{+2.2}_{-1.8}$
$B^+ \rightarrow D^+ K^{*0}$				
$K\pi\pi$	$-15.6^{+8.7}_{-7.1}$	463 ± 63	6338 ± 98	$-5.0^{+2.9}_{-2.1}$
$K_S^0\pi$	$-11.4^{+3.5}_{-2.4}$	35 ± 15	547 ± 27	$-33^{+10.2}_{-7.0}$
combined	-	-	-	$-5.3^{+2.3}_{-2.0}$

FIT PROCEDURE

The signal and background yields are extracted by maximizing the unbinned extended likelihood

$$\mathcal{L} = (e^{-N'} / N!) \cdot N'^N \cdot \prod_{j=1}^N f(\mathbf{x}_j | \theta, N'). \quad (1)$$

Here $\mathbf{x}_j = \{m_{\text{ES}}, \mathcal{F}\}$, θ is a set of parameters, N is the number of events in the selected sample, N' is the expectation value for the total number of events, and

$$f(\mathbf{x} | \theta, N') = \frac{N_{\text{sig}} f_{\text{sig}}(\mathbf{x} | \theta) + \sum_i N_{B_i} f_{B_i}(\mathbf{x} | \theta)}{N'}, \quad (2)$$

with $f_{\text{sig}}(\mathbf{x} | \theta)$ and $f_{B_i}(\mathbf{x} | \theta)$ the probability density functions (PDFs) for the hypothesis that the event is a signal or a background event, respectively. The B_i are the different background categories used in the fit: continuum background, combinatorial $B\bar{B}$ background, and peaking

$B\bar{B}$ background. N_{sig} is the number of signal events, and N_{B_i} is the number of events for each background species B_i .

The individual probability density functions are defined by the product of the one-dimensional distributions of m_{ES} and \mathcal{F} . Absence of the correlations between these distributions is checked using the MC samples. The signal m_{ES} distribution is modeled with a Gaussian function. The continuum and non-peaking $B\bar{B}$ background m_{ES} distributions are modeled with two different threshold ARGUS functions defined [13] as follows:

$$A(x) = x \sqrt{1 - \left(\frac{x}{x_0}\right)^2} \cdot e^{c \left(1 - \left(\frac{x}{x_0}\right)^2\right)}, \quad (3)$$

where x_0 represents the maximum allowed value for the variable x and c accounts for the shape of the distribution. The m_{ES} distribution of the peaking $B\bar{B}$ background is modeled with a Crystal Ball (CB) function

[14]. The CB function is a Gaussian modified to include a power-law tail on the low side of the peak. The \mathcal{F} distributions are modeled as the sum of two asymmetric Gaussians for signal and continuum background events, and with a Gaussian for the combinatorial $B\bar{B}$ background. For the peaking $B\bar{B}$ background we use a Gaussian distribution for the DK mode. For the DK^* mode, an asymmetric Gaussian is used for the $K\pi\pi$ mode and a sum of two asymmetric Gaussians for the $K_s^0\pi$ mode. The shape parameters of the threshold function for continuum background are determined from data. All other PDF parameters are derived from the simulated events.

In the fits we fix the numbers of peaking $B\bar{B}$ background events, which are estimated from the PDG branching fractions [11] and MC efficiency evaluations.

The number of signal events determined by the fit (N_{sig}) is used to calculate the branching fraction as

$$\mathcal{B}(B^+ \rightarrow D^+ K^0) = \frac{N_{\text{sig}}}{N_{B^+} \cdot \epsilon_{\text{sig}}} \cdot \frac{2}{\mathcal{B}_D \cdot \mathcal{B}_{K_s^0}},$$

where N_{B^+} is the total number of charged B mesons in the data sample (equal to the total number of all $B\bar{B}$ pairs produced, since we assume equal production of B^+B^- and $B^0\bar{B}^0$), \mathcal{B}_D and $\mathcal{B}_{K_s^0}$ are the branching fraction for each D meson decay channel and for $K_s^0 \rightarrow \pi^+\pi^-$ respectively [11], and ϵ_{sig} is the reconstruction efficiency for each D decay channel evaluated from MC events. The expression for $\mathcal{B}(B^+ \rightarrow D^+ K^{*0})$ is obtained replacing $\mathcal{B}_{K_s^0}/2$ with the branching fraction of $K^{*0} \rightarrow K^+\pi^-$, $\mathcal{B}_{K^{*0}}$. The likelihoods for individual channels are combined to derive average branching fractions for $B^+ \rightarrow D^+ K^0$ and $B^+ \rightarrow D^+ K^{*0}$.

The fit procedure is validated using an ensemble of simulated experiments (toy MC studies) with all yields generated according to Poisson distributions. The non-floating parameters of the fits as well as the shapes of the background threshold functions are fixed to the values obtained from the MC samples. We define the pull for a variable x as the difference between the fitted x_{fit} and the mean generated value $\langle x_{\text{gen}} \rangle$, divided by the error σ_{err} , $x_{\text{pull}} = (x_{\text{fit}} - \langle x_{\text{gen}} \rangle) / \sigma_{\text{err}}$. We use the negative errors for fitted values that are smaller than the generated ones and the positive errors in the opposite case. The procedure gives Gaussian-like pull distributions for each channel and thus no biases of the fit model were found. In Table III we show resulting expectations of asymmetric errors for each channel. The 95% probability ranges for these errors obtained from toy MC studies are also shown. Tests of the fit procedure performed on the full MC samples give values for the yields compatible with the generated ones.

The main results of the fit to the data are reported in Table IV, which gives the values of the fitted parameters for each D channel and for the combination of fits. The background yields are close to the expectations and the

errors obtained on the branching fractions are in good agreement with the values reported in Table III. The leading contribution (as expected) is obtained from the $K\pi\pi$ mode. Likelihood fit projections of the m_{ES} and \mathcal{F} distributions are shown in Fig. 2. In Fig. 3 we also show for illustrative purposes the fit projection for m_{ES} , after requiring $\mathcal{F} > 0$, to visually enhance any possible signal.

SYSTEMATIC ERRORS

We consider various sources of systematic error. One of the largest contributions comes from the uncertainties on the PDF parameterizations. To evaluate the contributions related to the m_{ES} and \mathcal{F} PDFs, we repeat the fit varying the MC-obtained PDF parameters within their statistical errors, taking into account correlations among the parameters (labeled as ‘‘PDF - MC’’ in the final list of systematic error sources). Differences between the data and MC (labeled as ‘‘Data - MC PDF shapes’’ in the final list of systematic error sources) for the shapes of m_{ES} and \mathcal{F} distributions are studied for signal components using data control samples. $\bar{B}^0 \rightarrow D^+\pi^-$ and $\bar{B}^0 \rightarrow D^+\rho^-$ selected events are used to obtain the m_{ES} and \mathcal{F} parameters for the DK and DK^* modes, respectively. The analysis strategy is the same as for the signal events except for specific criteria to select K_s^0 or K^{*0} . For the continuum background, we estimate this uncertainty by repeating the fit using the PDF parameters obtained from off-resonance data instead of those from continuum MC. Finally, for the $B\bar{B}$ background, we estimate this uncertainty by leaving the parameters that describe the $B\bar{B}$ combinatorial background as free variables in the fit (separately for m_{ES} and \mathcal{F}). The systematic uncertainty is defined as the difference in the branching fraction results from the nominal and alternative fits summed in quadrature.

The systematic errors on the signal reconstruction efficiency include the uncertainty due to limited MC statistics, uncertainties on possible differences between data and MC in tracking efficiency, K_s^0 and π^0 reconstruction, and charged-kaon identification. In addition, there are additional contributions to these uncertainties originating from the disagreement between data and MC distributions for all the variables used in the selection. These are estimated by comparing the data and simulation performance in control samples. To evaluate the uncertainties arising from peaking background contributions, we repeat the fit by varying the numbers of these events within their statistical errors. The uncertainties on the branching fractions of the sub-decay modes are also taken into account. The uncertainty on $N_{B\bar{B}}$ (1.1%) has a negligible effect on the total error.

The systematic uncertainties on the branching fractions are summarized in Table V. All the uncertainties are considered to be uncorrelated and are treated sepa-

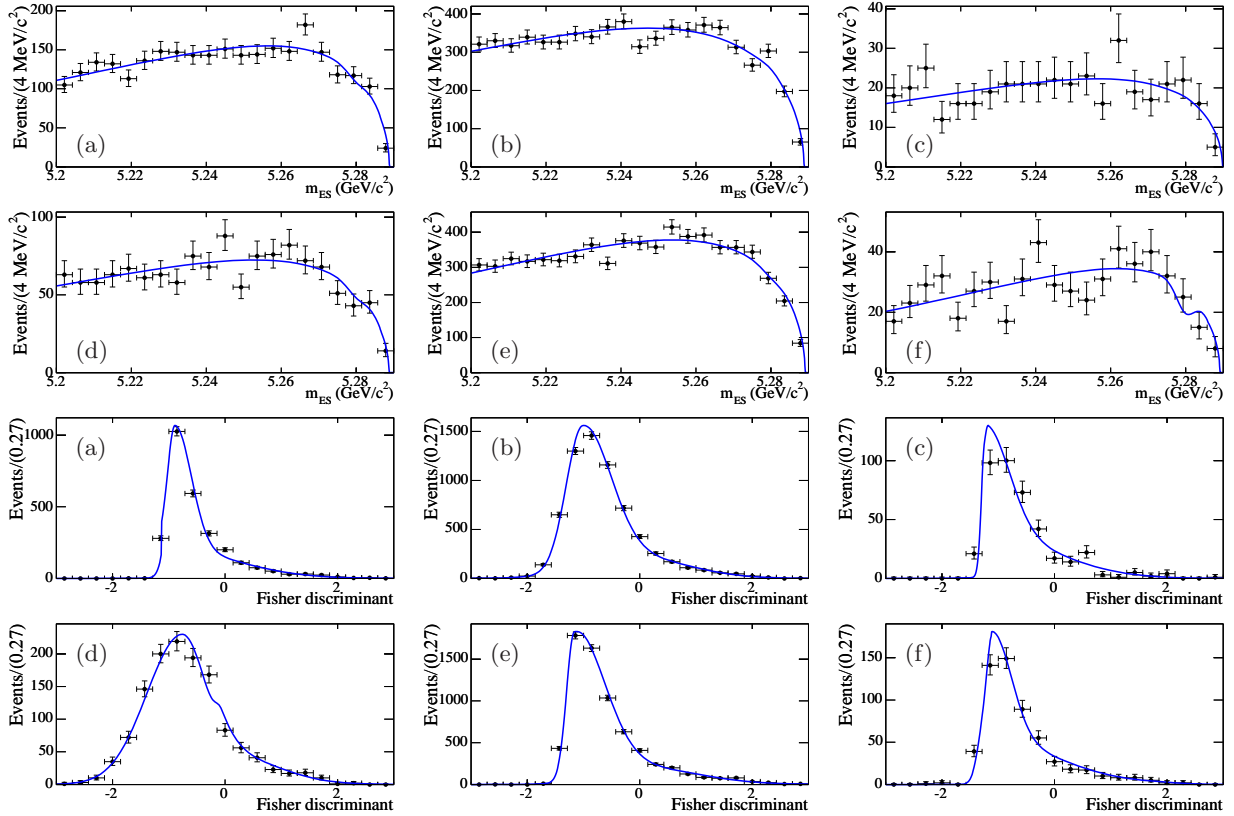


FIG. 2: (color online) Projections of the 2D likelihood function onto the m_{ES} (top two rows) and \mathcal{F} (bottom two rows) axes for (a) $K\pi\pi$, (b) $K\pi\pi\pi^0$, (c) $K_S^0\pi$ and (d) $K_S^0\pi\pi^0$ for the $B^+ \rightarrow D^+K_S^0$ mode, and (e) $K\pi\pi$ and (f) $K_S^0\pi$ for the $B^+ \rightarrow D^+K^{*0}$ mode. The data are indicated with black dots and error bars and the (blue) solid curve is the projection of the fit.

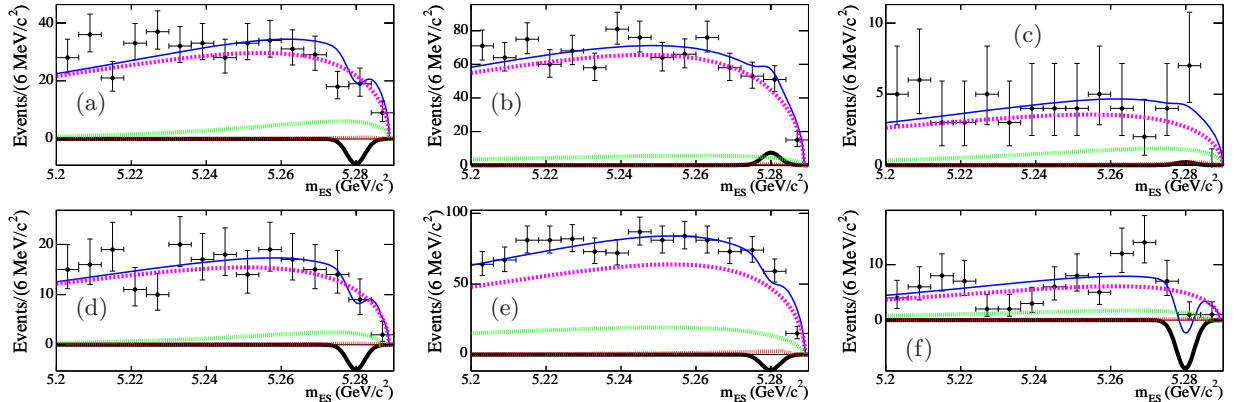


FIG. 3: (color online) From top left to bottom right: m_{ES} projection for (a) $K\pi\pi$, (b) $K\pi\pi\pi^0$, (c) $K_S^0\pi$, and (d) $K_S^0\pi\pi^0$ for the $B^+ \rightarrow D^+K_S^0$ mode and (e) $K\pi\pi$ and (f) $K_S^0\pi$ for the $B^+ \rightarrow D^+K^{*0}$ mode. The data are indicated with black dots and error bars and the different fit components are shown: signal (black solid curve), combinatorial $B\bar{B}$ (green dotted), continuum (magenta dot-dashed) and $B\bar{B}$ peaking background (red dotted) and the blue solid curve is the projection of the fit. We require $\mathcal{F} > 0$ to visually enhance the signal. Such a cut has an approximate efficiency of 70% for signal, while it rejects more than 80% of the continuum background.

rately for each channel.

RESULTS FOR BRANCHING FRACTIONS

The final likelihood for each decay mode is obtained by convolving the likelihoods for the measured branching fractions with Gaussian functions of width equal to the systematic uncertainty.

The final results including systematic uncertainties are

$$\begin{aligned}\mathcal{B}(B^+ \rightarrow D^+ K^0) &= (-3.8^{+2.5}_{-2.4}) \times 10^{-6}, \\ \mathcal{B}(B^+ \rightarrow D^+ K^{*0}) &= (-5.3 \pm 2.7) \times 10^{-6}.\end{aligned}$$

Since the measurements for the branching fractions are not statistically significant, following a Bayesian approach and assuming a flat prior distribution for the branching fractions, we integrate over the positive portion of the likelihood function to obtain the following upper limits at 90% probability:

$$\begin{aligned}\mathcal{B}(B^+ \rightarrow D^+ K^0) &< 2.9 \times 10^{-6}, \\ \mathcal{B}(B^+ \rightarrow D^+ K^{*0}) &< 3.0 \times 10^{-6}.\end{aligned}$$

The $B^+ \rightarrow D^+ K^0$ result represents an improvement over, and supersedes, our previous result [7], while the $B^+ \rightarrow D^+ K^{*0}$ result is the first for this channel.

CONCLUSIONS

In summary, we have presented a search for the rare decays $B^+ \rightarrow D^+ K^0$ and $B^+ \rightarrow D^+ K^{*0}$, which are predicted to proceed through annihilation or rescattering amplitudes. We do not observe any significant signal and we set 90% probability upper limits on their branching fractions.

ACKNOWLEDGMENTS

We are grateful for the extraordinary contributions of our PEP-II colleagues in achieving the excellent luminosity and machine conditions that have made this work possible. The success of this project also relies critically on the expertise and dedication of the computing organizations that support *BABAR*. The collaborating institutions wish to thank SLAC for its support and the kind hospitality extended to them. This work is supported by the US Department of Energy and National Science Foundation, the Natural Sciences and Engineering Research Council (Canada), the Commissariat à l'Énergie Atomique and

Institut National de Physique Nucléaire et de Physique des Particules (France), the Bundesministerium für Bildung und Forschung und Deutsche Forschungsgemeinschaft (Germany), the Istituto Nazionale di Fisica Nucleare (Italy), the Foundation for Fundamental Research on Matter (The Netherlands), the Research Council of Norway, the Ministry of Education and Science of the Russian Federation, Ministerio de Ciencia e Innovación (Spain), and the Science and Technology Facilities Council (United Kingdom). Individuals have received support from the Marie-Curie IEF program (European Union), the A. P. Sloan Foundation (USA) and the Binational Science Foundation (USA-Israel).

* Now at Temple University, Philadelphia, Pennsylvania 19122, USA

† Also with Università di Perugia, Dipartimento di Fisica, Perugia, Italy

‡ Also with Università di Roma La Sapienza, I-00185 Roma, Italy

§ Now at University of South Alabama, Mobile, Alabama 36688, USA

¶ Also with Università di Sassari, Sassari, Italy

- [1] A. J. Buras and L. Silvestrini, Nucl. Phys. B **569**, 3 (2000).
- [2] B. Blok, M. Gronau, and J.L. Rosner, Phys. Rev. Lett. **78** 3999 (1997).
- [3] B. Aubert *et al.* [*BABAR* Collaboration], Phys. Rev. D **76**, 052002 (2007); B. Aubert *et al.* [*BABAR* Collaboration], Phys. Rev. D **77**, 011107 (2008); K. Ikado *et al.*, Phys. Rev. Lett. **97**, 251802 (2006).
- [4] Charge conjugation is implied throughout this paper.
- [5] G. Cavoto *et al.*, Proceedings of the CKM 2005 Workshop (WG5), UC San Diego, 15-18 March 2005 [arXiv:hep-ph/0603019].
- [6] M. Gronau and D. London, Phys. Lett. B **253**, 483 (1991).
- [7] B. Aubert *et al.* (*BABAR* Collaboration), Phys. Rev. D **72**, 011102 (2005).
- [8] B. Aubert *et al.* [*BABAR* Collaboration], Phys. Rev. D **66**, 032003 (2002).
- [9] *PEP II - An Asymmetric B Factory, Conceptual Design Report*, SLAC-418, LBL-5379 (1993).
- [10] B. Aubert *et al.* (*BABAR* Collaboration), Nucl. Instr. and Methods A **479**, 1 (2002).
- [11] C. Amsler *et al.* (Particle Data Group), Phys. Lett. B **667**, 1 (2008).
- [12] R. A. Fisher, Annals Eugen. **7**, 179 (1936).
- [13] H. Albrecht *et al.* (ARGUS Collaboration), Z. Phys. C **48**, 543 (1990).
- [14] J. E. Gaiser, Ph.D. thesis, Stanford University [SLAC-R-255] (1982).

TABLE V: Systematic errors on branching fractions for $B^+ \rightarrow D^+ K^0$ and $B^+ \rightarrow D^+ K^{*0}$ decay channels. All quantities are given in units of 10^{-6} .

	$B^+ \rightarrow D^+ K^0$				$B^+ \rightarrow D^+ K^{*0}$	
	$K\pi\pi$	$K\pi\pi\pi^0$	$K_S^0\pi$	$K_S^0\pi\pi^0$	$K\pi\pi$	$K_S^0\pi$
PDF - MC	+0.8 -0.8	+6.2 -3.4	+5.3 -4.4	+7.3 -8.8	+0.6 -0.9	+3.1 -3.6
Data-MC PDF shapes:						
Continuum background	0.2	0.4	1.4	0.5	0.1	1.7
$B\bar{B}$ background	0.7	1.6	2.5	5.0	1.0	4.4
Signal	< 0.05	9.2	5.6	0.9	0.9	3.1
Efficiency error:						
Reconstruction efficiency (MC)	0.1	0.6	< 0.05	0.9	0.1	0.5
Data-MC	0.2	0.8	< 0.05	0.5	0.2	0.3
Peaking background	< 0.05	0.5	0.2	0.2	< 0.05	0.1
\mathcal{B} errors	0.3	0.3	< 0.05	0.4	< 0.05	0.1
Combined	+1.1 -1.3	+11.3 -11.8	+8.2 -9.3	+9.0 -12.5	+1.5 -1.8	+6.4 -7.4